J|A|C|S
ARTICLES
Published on Web 12/21/2006

CT−CT Annihilation in Rigid Perylene End-Capped Pentaphenylenes

Eduard Fron,[†] Toby D. M. Bell,[‡] Antoine Van Vooren,[§] Gerd Schweitzer,[†] Jérôme Cornil,[§] David Beljonne,[§] Paul Toele,[†] Josemon Jacob,[||] Klaus Müllen,[||] Johan Hofkens,[†] Mark Van der Auweraer,[†] and Frans C. De Schryver*[,†]

Contribution from the Department of Chemistry and Institute of Nanoscale Physics and Chemistry, Katholieke Universiteit Leuven, Celestijnenlaan 200 F, 3001 Heverlee, Belgium, School of Chemistry, University of Melbourne, Parkville 3010, Australia, Laboratory for Chemistry of Novel Materials, University of Mons-Hainaut, Place du Parc 20, B-7000 Mons, Belgium, and Max Planck Institute for Polymer Research, Ackermannstrasse 10, 55128 Mainz, Germany

Received July 25, 2006; E-mail: Frans.DeSchryver@chem.kuleuven.be

Abstract: The time-dependent spectral properties of a rigid, extended system consisting of three pentaphenylene units end-capped with perylene monoimide were investigated in detail by femtosecond transient absorption and single photon timing measurements. In polar solvents, the molecular system shows the occurrence of photoinduced charge transfer. Upon gradually increasing the excitation power, annihilation involving two states with charge-transfer character has been observed. Quantum-chemical calculations performed on the system consisting of two pentaphenylene units end-capped with perylene monoimide strongly support the experimental data.

Introduction

In recent years, much effort has been directed toward incorporating various members of the perylene dye family into different molecular assemblies to study intramolecular photoinduced electron and energy-transfer processes.[1,2] The aim for such studies is threefold: (i) to design molecular systems in which the visible light is captured, transported, and converted into chemical energy mimicking the reaction center in photosynthesis,[3,4] (ii) to reveal fundamental details of how these elementary processes occur, and (iii) to obtain organic assemblies such as organic oligomers and perylene-based polymers which are potential active materials in solar cells.[5] Considerable attention has been paid to develop synthetic molecular architectures containing chromophores separated by rigid spacers with well-defined lengths showing fluorescence resonance energy transfer (FRET).[6−8]

Several studies on various processes taking place in dendritic mono- or multichromophoric structures provide information of the excited-state kinetic properties of the peryleneimide (**PI**) chromophore with respect to electronic energy transfer and photoinduced electron transfer.[9−15]

Recent experimental investigations in a series of **PI**-based bichromophoric systems with fluorene trimers and hexamers as spacers have revealed the existence of three energy-transfer pathways, namely, energy hopping, singlet−singlet (S−S), and singlet−triplet (S−T) annihilation.[16−19] Similar kinetic pathways

[†] Katholieke Universiteit Leuven.
[‡] University of Melbourne.
[§] University of Mons-Hainaut.
[||] Max Planck Institute for Polymer Research.

(1) (a) Prodi, A.; Chiorboli, C.; Scandola, F.; Iengo, E.; Alessio, E.; Dobrawa, R.; Würthner, F. *J. Am. Chem. Soc.* **2005**, *127*, 1454−1462. (b) Würthner, F.; You, C. C.; Saha-Möller, C. *Chem. Soc. Rev.* **2004**, *33*, 133−146.
(2) Lor, M.; Viaene L.; Pilot, R.; Fron, E.; Jordens, S.; Schweitzer, G.; Weil, T.; Müllen, K.; Verhoeven, J. W.; Van der Auweraer, M.; De Schryver, F. C. *J. Phys. Chem. B* **2004**, *108*, 10721−10731.
(3) McDermott, G.; Prince, S. M.; Freer, A. A.; Hawthornthwaite-Lawless, A. M.; Papiz, M. Z.; Cogdell, R. J.; Isaacs, N. W. *Nature* **1995**, *374*, 517−521.
(4) Kühlbrandt, W.; Wang, D. N. *Nature* **1991**, *350*, 130−134.
(5) Brabec, C. J.; Sariciftci, N. S.; Hummelen, J. C. *Adv. Funct. Mater.* **2001**, *11*, 15−26.
(6) De Schryver, F. C.; Vosch, T.; Cotlet, M.; Van der Auweraer, M.; Müllen, K.; Hofkens, J. *Acc. Chem. Res.* **2005**, *38*, 514−522.
(7) Jordens, S.; De Belder, G.; Lor, M.; Schweitzer, G.; Van der Auweraer, M.; Weil, T.; Reuther, E.; Müllen, K.; De Schryver, F. C. *Photochem. Photobiol. Sci.* **2003**, *2*, 177−186.
(8) Muls, B.; Uji-i, H.; Melnikov, S.; Moussa, A.; Verheijen, W.; Soumillion, J. P.; Josemon, J.; Müllen, K.; Hofkens, J. *Chem. Phys. Chem.* **2005**, *6*, 2286−2294.
(9) Lor, M.; Jordens, S.; De Belder, G.; Schweitzer, G.; Fron, E.; Viaene, L.; Cotlet, M.; Weil, T.; Müllen, K.; Verhoeven, J. W.; Van der Auweraer, M.; De Schryver, F. C. *Photochem. Photophys. Sci.* **2003**, *2*, 501−510.
(10) Jordens, S.; De Belder, G.; Lor, M.; Schweitzer, G.; Van der Auweraer, M.; Weil, T.; Herrmann, A.; Wiesler, U. M.; Müllen, K.; De Schryver, F. C. *Photochem. Photobiol. Sci.* **2003**, *2*, 1118−1124.
(11) Lor, M.; Thielemans, J.; Viaene, L.; Cotlet, M.; Hofkens, J.; Weil, T.; Hampel, C.; Müllen, K.; Verhoeven, J. W.; Van der Auweraer, M.; De Schryver, F. C. *J. Am. Chem. Soc.* **2002**, *124*, 9918−9925.
(12) De Belder, G.; Schweitzer, G.; Jordens, S.; Lor, M.; Mitra, S.; Hofkens, J.; De Feyter, S.; Van der Auweraer, M.; Herrmann, A.; Weil, T.; Müllen, K.; De Schryver, F. C. *Chem. Phys. Chem.* **2001**, *2*, 49−55.
(13) Vosch, T.; Cotlet, M.; Hofkens, J.; Van Der Biest, K.; Lor, M.; Weston, K.; Tinnefeld, P.; Sauer, M.; Latterini, L.; Müllen, K.; De Schryver, F. C. *Phys. Chem.* **2003**, *107*, 6920−6931.
(14) Maus, M.; Mitra, S.; Lor, M.; Hofkens, J.; Weil, T.; Herrmann, A.; Müllen, K.; De Schryver, F. C. *J. Phys. Chem. A* **2001**, *105*, 3961−3966.
(15) Karni, Y.; Jordens, S.; De Belder, G.; Schweitzer, G.; Hofkens, J.; Gensch, T.; Maus, M.; De Schryver, F. C.; Hermann, A.; Müllen, K. *Chem. Phys. Lett.* **1999**, *310*, 73−78.
(16) Hofkens, J.; Cotlet, M.; Vosch, T.; Tinnefeld, P.; Weston, K. D.; Ego, C.; Grimsdale, A.; Müllen, K.; Beljonne, D.; Brédas, J. L.; Jordens, S.; Schweitzer, G.; Sauer, M.; De Schryver, F. C. *Proc. Natl. Acad. Sci. U.S.A.* **2003**, *100*, 13146−13151.

 10.1021/ja064794e CCC: $37.00

are possible in molecules containing excitation donor/acceptor pairs and in natural and synthetic multichromophoric systems such as light-harvesting antenna, fluorescent proteins, polymers, and dendrimers.[20−32] The relative contributions of these energy-transfer pathways to the photophysics of the systems are mainly determined by the spectroscopic properties of the active chromphores, their relative geometrical configuration, and the absorbed light intensity.

Due to its excellent stability, high quantum yield of fluorescence, and a large molar extinction coefficient, a **PI** dye has been used to functionalize a polyphenylene (**pPh**) unit, which emits in the blue, to tune the emission across the visible range.[33,34] In a previous study, a compound based on a **PI** attached to a **pPh** moiety embedded in a polymethyl methacrylate (PMMA) matrix showed a switching of the emission from the locally excited state to the charge transfer (CT) state.[35] By applying quantum-chemical methods to this molecular system in a polar solvent, it has been found that the CT state adopts a planar geometry in contrast to the twisted ground-state geometry in the gas phase.[36]

A rigid, extended system consisting of three pentaphenylene moieties end-capped with **PI**, here **PI-(pPh)$_3$-PI** and the analogous system **PI-(pPh)$_2$** containing a single **PI** unit and two (**pPh**) moieties (Scheme 1), is investigated in this study. The pentaphenylene linear backbone **(pPh)$_3$**, which is about 6 nm long, has mainly two functions: serving as electron donor unit and as a rigid bridge keeping both chromophores at a well-defined distance and within a nearly collinear orientation. Photon antibunching measurement results on single molecules of **PI-(pPh)$_3$-PI** embedded in PMMA films indicated that this system

Scheme 1. Molecular Structures of **PI-(pPh)$_2$** (**1**) and **PI-(pPh)$_3$-PI** (**2**); R = *n*-octyl, Ar = 4-*n*-octylphenyl

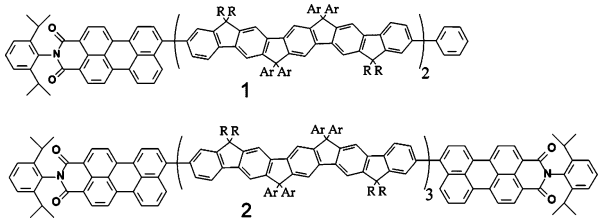

is a highly efficient, deterministic single photon source at room temperature.[27] This phenomenon was suggested to be due to an excited-state annihilation event involving two charge transfer states where **pPh**s and **PI**s act as electron donor and electron acceptor, respectively. To fully understand and reveal the influence of the CT, we have studied the excited-state behavior of the ensemble on a picosecond time scale.

Experimental Section

Materials and Steady-State Measurements. The synthesis of the stiff triple pentaphenylene blocks **(pPh)$_3$** end-capped with two perylene monoimide chromphores (**PI**) and the compound **PI-(pPh)$_2$** was published previously.[27] The **PI-(pPh)$_2$** sample contains a small fraction of **PI-(pPh)$_1$** that does not affect the photophysics of **PI-(pPh)$_2$** investigated in this study. The electron donor/acceptor capacity of the **pPh** and **PI** moieties is given by the value of the oxidation potential (E_{ox} = 1.31 V) and the reduction potential (E_{red} = −0.875 V, both measured versus Ag/AgCl with a ferrocene/ferrocenium internal standard in acetonitrile solution containing 0.1 M tetrabutylammonium perchlorate), respectively.[33]

The steady-state absorption spectra were recorded on a Lambda 40 spectrophotometer (Perkin-Elmer), and the fluorescence emission spectra were recorded on a Fluorolog I fluorimeter (SPEX). To study the kinetic processes in solvents of different polarity, **PI-(pPh)$_2$** and **PI-(pPh)$_3$-PI** were investigated in methylcyclohexane (MCH), tetralin, tetrahydrofuran (THF), and benzonitrile (PhCN).[37] These solvents provided by Aldrich were spectroscopic grade 99% and used as received. For the fluorescence experiments, the optical density of all solutions was kept below 0.1 at the absorption maximum in a 1-cm cuvette. The excitation wavelength was set to 495 nm. The fluorescence quantum yields of the two compounds were determined using rhodamine B in ethanol as a reference (for λ_{ex} = 495 nm).[38]

Time-Resolved Experiments. The picosecond fluorescence measurements of **PI-(pPh)$_2$** and **PI-(pPh)$_3$-PI** were performed in MCH, tetralin, and THF as solvents of different polarity using the single photon timing technique. All measurements were done with excitation at 483 nm in 1-cm cuvettes (OD ≈ 0.1), detected with 6 ps/ch resolution and globally analyzed taking into account the system prompt response of 40 ps.[39] In the femtosecond transient absorption setup, deoxygenated samples were excited at 580 nm in 1-mm cuvettes (OD ≈ 0.4) such that multichromophore excitation was possible (for details, see Supporting Information, SI). Probing was done under magic angle conditions in time windows of 50, 420, and 1400 ps. All data were commonly treated in a global analysis, taking into account the system prompt of ca. 300 fs.[40] In the power dependence series, the laser power in the 80 μm focus was set to 340, 120, 90, 60, and 45 μW, all of which were out of the saturation level.

(17) Beljonne, D.; Pourtois, G.; Silva, C.; Hennebicq, E.; Herz, L. M.; Friend, R. H.; Scholes, G. D.; Setayesh, S.; Müllen, K.; Brédas, J. L. *Proc. Natl. Acad. Sci. U.S.A.* **2002**, *99*, 10982−10987.
(18) Beljonne, D.; Pourtois, G.; Shuai, Z.; Hennebicq, E.; Scholes, G. D.; Brédas, J. L. *Synth. Met.* **2003**, *137*, 1369−1371.
(19) Hennebicq, E.; Pourtois, G.; Scholes, G. D.; Herz, L. M.; Russell, D. M.; Silva, C.; Setayesh, S.; Grimsdale, A. C.; Müllen, K.; Brédas, J. L.; Beljonne, D. *J. Am. Chem. Soc.* **2005**, *127*, 4744−4762.
(20) VandenBout, D. A.; Yip, W. T.; Hu, D. H.; Fu, D. K.; Swager, T. M.; Barbara, P. F. *Science* **1997**, *277*, 1074−1077.
(21) (a) Yu, J.; Hu, D. H.; Barbara, P. F. *Science* **2000**, *289*, 1327−1330. (b) Scholes, G. D. *Annu. Rev. Phys. Chem.* **2003**, *54*, 57−87.
(22) Tinnefeld, P.; Herten, D. P.; Sauer, M. *J. Phys. Chem. A* **2001**, *105*, 7989−8003.
(23) Vosch, T.; Cotlet, M.; Hofkens, J.; Van Der Biest, K.; Lor, M.; Weston, K.; Tinnefeld, P.; Sauer, M.; Latterini, L.; Müllen, K.; De Schryver, F. C. *J. Phys. Chem. A* **2003**, *107*, 6920−6931.
(24) Van Oijen, A. M.; Ketelaars, M.; Köhler, J.; Aartsma, T. J.; Schmidt, J. *Science* **1999**, *285*, 400−402.
(25) Bopp, M. A.; Jia, Y. W.; Li, L. Q.; Cogdell, R. J.; Hochstrasser, R. M. *Proc. Natl. Acad. Sci. U.S.A.* **1997**, *94*, 10630−1063.
(26) Cotlet, M.; Hofkens, J.; Habuchi, S.; Dirix, G.; Van Guyse, M.; Michiels, J.; Vanderleyden, J.; De Schryver, F. C. *Proc. Natl. Acad. Sci. U.S.A.* **2001**, *98*, 14398−14403.
(27) Bell, T. D. M.; Jacob, J.; Izguierdo, M. A.; Fron, E.; Nolde, F.; Hofkens, J.; Müllen, K.; De Schryver, F. C. *Chem. Commun.* **2005**, *39*, 4973−4975.
(28) Gesquiere, A. J.; Uwada, T.; Asahi, T.; Masuhara, H.; Barbara, P. F. *Nano Lett.* **2005**, *5*, 1321.
(29) Grey, J. K.; Kim, D. Y.; Donley, C. L.; Miller, W. L.; Kim, J. S.; Silva, C.; Friend, R. H.; Barbara, P. F. *J. Phys. Chem. B* **2006**, *110*, 18898−18903.
(30) Becker, K.; Lupton, J. M. *J. Am. Chem. Soc.* **2006**, *128*, 6468−6479.
(31) Becker, K.; Lupton, J. M.; Feldmann, J.; Setayesh, S.; Grimsdale, A. C.; Müllen, K. *J. Am. Chem. Soc.* **2006**, *128*, 680−681.
(32) Watson, M. D.; Fechtenkötter, A.; Müllen, K. *Chem. Rev.* **2001**, *101*, 1267−1300.
(33) Jacob, J.; Sax, S.; Piok, T.; List, E. J. W.; Grimsdale, A. C.; Müllen, K. *J. Am. Chem. Soc.* **2004**, *126*, 6987−6995.
(34) Hofkens, J.; Maus, M.; Gensch, T.; Vosch, T.; Cotlet, M.; Köhn, F.; Herrmann, A.; Müllen, K.; De Schryver, F. C. *J. Am. Chem. Soc.* **2000**, *122*, 9278.
(35) Izquierdo, M. A.; Bell, T. D. M.; Satoshi, H.; Fron, E.; Pilot, R.; Vosch, T.; De Feyter, S.; Verhoeven, J.; Jacob, J.; Müllen, K.; Hofkens, J.; De Schryver, F. C. *Chem. Phys. Lett.* **2005**, *401*, 503−508.
(36) Sun, M. *Chem. Phys. Lett.* **2005**, *408*, 128−133.
(37) *CRC Handbook of Physics and Chemistry*, 73rd ed.; Lide, D. R., Ed.; CRC Press: Boca Raton, FL, 1992.
(38) Du, H.; Fuh, R. A.; Li, J.; Corkan, A.; Lindsey, J. S. *Photochem. Photobiol.* **1998**, *68*, 141−142.
(39) Maus, M.; Rousseau, E.; Cotlet, M.; Schweitzer, G.; Hofkens, J.; Van der Auweraer, M.; De Schryver, F. C. *Rev. Sci. Instrum.* **2001**, *72*, 36−40.
(40) Schweitzer, G.; Xu, L.; Craig, B.; De Schryver, F. C. *Opt. Commun.* **1997**, *142*, 283−288.

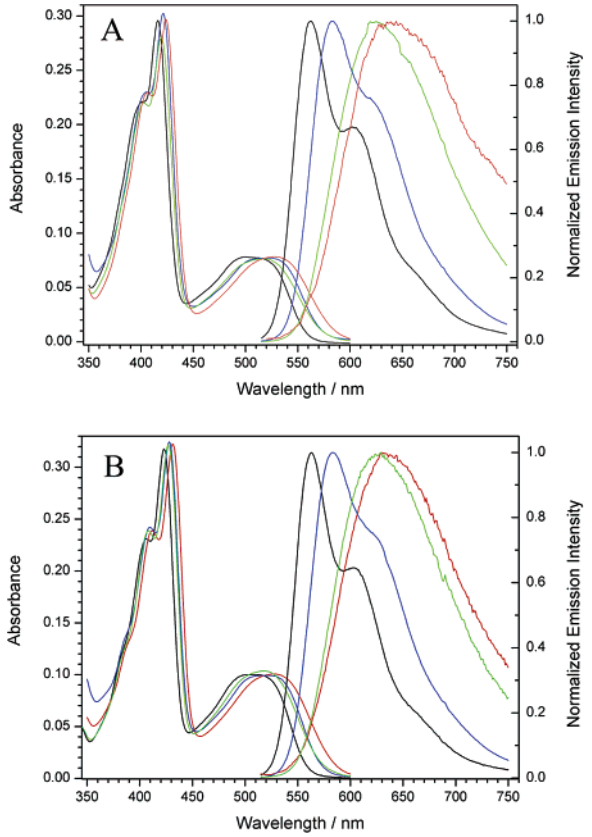

Figure 1. (A) Normalized absorption and emission spectra (excitation at 495 nm) of the compound **PI-(pPh)$_2$** in MCH (black), tetralin (blue), and THF (green). (B) Normalized absorption and emission spectra (excitation at 495 nm) of the compound **PI-(pPh)$_3$-PI** in MCH (black), tetralin (blue), THF (green), and PhCN (red).

Quantum-Chemical Calculations Methodology. The ground-state and excited-state geometries of the model compound for **PI-(pPh)$_3$-PI**, that is, **PI-(pPh)$_3$**, were optimized at the AM1 and AM1-CI levels, respectively.[41] On the basis of these geometries, intermediate neglect of differential overlap (INDO)/single configuration interaction (SCI) and INDO/coupled cluster singles and doubles (CCSD) calculations were performed to assess the nature and localization of the lowest singlet excited state.[42,43] To depict electron−electron interactions, a screened Mataga−Nishimoto potential was used: $V_{SCR}(r) = V_{MN}(\sigma r)$ where σ is a factor that was tuned to reproduce the observed shift in fluorescence maximum with solvent polarity ($\sigma = 1$ corresponds to the gas phase).[44] Such screened potentials yielded a better description of CT-like electronic excitations in conjugated polymers as they accounted for polarization phenomena in the condensed phase.[45] Although σ in principle only considered the high-frequency dielectric constant ($\epsilon_r(\infty)$), it was also able to estimate the stabilization of a CT-like state by interaction with the orientational polarization ($\epsilon_r(0)$) induced by this charge transfer.

Results

Steady-State Measurements. Figure 1 displays the normalized steady-state absorption and emission spectra of the **PI-(pPh)$_2$** and **PI-(pPh)$_3$-PI** in solvents of different polarity as indicated. The fluorescence quantum yields measured in degassed conditions are compiled in Table 1. The extinction coefficient of **PI-(pPh)$_2$** was measured in toluene and amounts to 52 000 M^{-1} cm^{-1} at 515 nm, being 37% higher than that for **C1P1** (structure shown in SI Scheme 1), whose extinction coefficient is 38 000 M^{-1} cm^{-1} at 490 nm and $\Phi_f = 0.95$ in toluene.

Table 1. Fluorescence Quantum Yields of the Compounds **PI-(pPh)$_2$** and **PI-(pPh)$_3$-PI** in Four Solvents of Different Polarity[a]

compound	MCH ($\epsilon = 2.02$)	tetralin ($\epsilon = 2.73$)	THF ($\epsilon = 7.6$)	PhCN ($\epsilon = 25.2$)
PI-(pPh)$_2$	0.80	0.53	0.35	0.06
PI-(pPh)$_3$-PI	0.73	0.56	0.26	0.02

[a] The values of the dielectric constants, ϵ, are taken from ref 37.

Single Photon Timing and Polychromatic Femtosecond Transient Absorption Measurements. PI-(pPh)$_2$. MCH and Tetralin. By SPT experiments in MCH, the fluorescence intensity of **PI-(pPh)$_2$** was found to decay monoexponentially with a time constant of 2.8 ns (3.5×10^8 s^{-1}). Combined with the fluorescence quantum yield of 0.80, this yields a fluorescent rate constant of 2.8×10^8 s^{-1}. Time-resolved transient absorption spectra obtained upon excitation at 495 nm (400 μW excitation power) are depicted in Figure 2A. From the 50-ps time window, another two additional components were precisely retrieved: a fast decay time of 4.2−5 ps attributed to a vibrational relaxation process also found in similar compounds containing the peryleneimide chromophore as, for example, **C1P1**[9,11,46] (structure shown in SI Scheme 1) and an ultrafast time constant of 0.5−2 ps attributed to intramolecular vibrational redistribution (IVR).[47] These last two kinetic components were found in all femtosecond data but are not highlighted here because they are out of the scope of this article. In another series of measurements, power-dependent excitation experiments have been performed. The transient absorption measurements carried out at 60 and 400 μW excitation powers confirmed no difference in decay traces recorded in the 50- and 420-ps time windows (data not shown).

By SPT measurements in tetralin, **PI-(pPh)$_2$** was found to decay with 50 ps and 2.6 ns time constants (9 and 91% amplitude, respectively, at 580-nm detection wavelength). In addition to components attributed to IVR and vibrational relaxation, the kinetic analysis of the femtosecond transient absorption data of **PI-(pPh)$_2$** in tetralin revealed two components with decay time constants of 52 ps (1.9×10^{10} s^{-1}) and 2.6 ns (3.8×10^8 s^{-1}).

THF. SPT experiments showed that **PI-(pPh)$_2$** in THF decays biexponentially with a long time constant of 2.2 ns (0.45×10^9 s^{-1}) and a very short one (<30 ps) below the temporal resolution of the setup. Figure 2B displays the three-dimensional plot of the transient absorption spectra in THF recorded in a 50-ps time window (400 μW excitation power). This spectrum differs clearly from those obtained in MCH and tetralin. By global kinetic analysis of these decay traces in addition to components attributed to IVR and vibrational relaxation, two additional time components with decay times of 6 ps (1.66×10^{11} s^{-1}) and 2.2 ns (4.5×10^8 s^{-1}) were found. An additional series of

(41) Semichem, Inc.: Shawnee, KS, 1997.
(42) Seminario, J. M.; Zacarias, A. G.; Tour, J. M. *J. Am. Chem. Soc.* **2000**, *122*, 3015−3020.
(43) Shuai, Z.; Brédas, J. L. *Phys. Rev. B* **2000**, *62*, 15452−15460.
(44) Mataga, N.; Nishimoto, K. *Z. Chem. Phys.* **1957**, *13*, 140.
(45) Chandross, M.; Mazumdar, S. *Phys. Rev. B* **1997**, *55*, 1497−1504.
(46) Fron, E.; Lor, M.; Pilot, R.; Schweitzer, G.; Dincalp, H.; De Feyter, S.; Cremer, J.; Bäuerle, P.; Müllen, K.; Van der Auweraer, M.; De Schryver, F. C. *Photochem. Photobiol. Sci.* **2005**, *4*, 61−68.
(47) De Belder, G.; Schweitzer, G.; Jordens, S.; Lor, M.; Mitra, S.; Hofkens, J.; De Feyter, S.; Van der Auweraer, M.; Hermann, A.; Weil, T.; Müllen, K.; De Schryver, F. C. *ChemPhysChem* **2001**, *1*, 49−55.

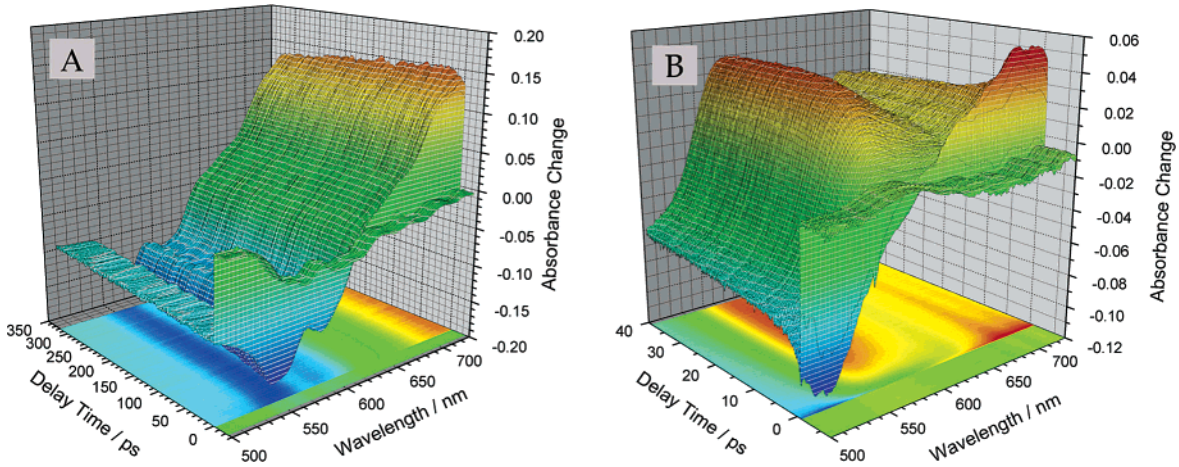

Figure 2. Three-dimensional plot of the femtosecond transient absorption spectra of **PI-(pPh)$_2$** in MCH (A) recorded within a 420-ps time window and in THF (B) recorded within a 50-ps time window.

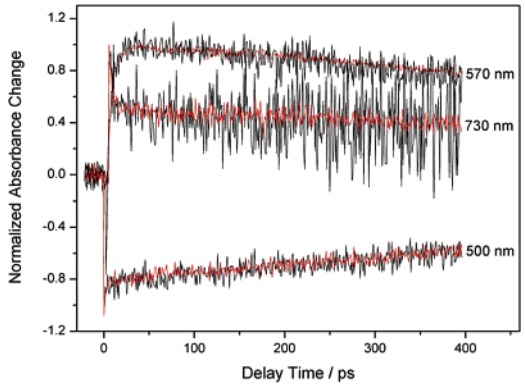

Figure 3. Femtosecond transient absorption decay traces of **PI-(pPh)$_2$** in THF recorded with excitation power of 60 μW (black) and 400 μW (red) in a 420-ps time window. The wavelengths were selected according to the regions of interest.

experiments was performed with two different excitation powers of 60 and 400 μW in time windows of 50 and 420 ps. Figure 3 shows a comparison of the traces recorded with these two excitation powers. Similarly to the observation for experiments in MCH and tetralin (data not shown), the variation of the excitation power shows no difference in decay behavior of **PI-(pPh)$_2$**.

PI-(pPh)$_3$-PI. MCH and Tetralin. SPT experiments on **PI-(pPh)$_3$-PI** in MCH recorded fluorescence decay traces that could be fitted monoexponentially with a decay time of 2.7 ns (3.7×10^8 s^{-1}). The three-dimensional plot of the femtosecond transient absorption spectra looks similar to that of **PI-(pPh)$_2$** in the same solvent (Figure 4A). In addition to a component with a long decay time, corresponding to that found in SPT, the femtosecond data revealed components attributed to IVR and vibrational relaxation found also in **PI-(pPh)$_2$**. Comparing the decay traces recorded with 60, 120, and 340 μW (Figure 4B), a good match of the traces is found, suggesting no influence of the excitation power change on the decay times in both the negative and positive bands (see SI Figure 1 for time-resolved transient absorption traces and the wavelength dependency of the partial amplitudes).

From the transient absorption experiments of **PI-(pPh)$_3$-PI** in tetralin, two components with decay times of 50 ps (1.9×10^{10} s^{-1}) and 2.6 ns (3.8×10^8 s^{-1}) were identified from the kinetic analysis. Furthermore, the evolution in time of a few selected spectra clearly illustrates that the maximum of the stimulated emission shifts from an initial value of 560 to 580 nm in a time span of 50 to 100 ps. No excitation power dependency could be found (for details, see SI Figure 2).

THF. PI-(pPh)$_3$-PI resembles the kinetic behavior of **PI-(pPh)$_2$** to a certain extent when both are measured in THF. When analyzing the fluorescence decays obtained by SPT, a long decay component of 2.2 ns is found together with a very short one (<30 ps) unresolved due the limited resolution of the setup. Figure 5 shows a comparison of the three-dimensional plot of the femtosecond transient absorption spectra of **PI-(pPh)$_3$-PI** in THF recorded with 45 and 120 μW excitation power. A faster decay in both the negative band centered at 520 nm and the positive band centered at 570 nm is already observable upon a 3-fold increase in the excitation power (Figure 5).

Stepwise changing the excitation power impinging on the sample from 45 to 60, 90, 120, and 340 μW leads to a clear and systematic difference within the series of decays at 510 (ground-state depletion) and 570 nm (induced emission), while no change in the absorption signal situated at 730 nm (Figure 5 C) is observed.

In the analysis of the decay traces of the femtosecond transient absorption data obtained at low excitation power (45 μW), in addition to the IVR and vibrational relaxation, two components with decay times of 6 ps and 2.2 ns were recovered. A similar type of kinetic analysis was carried out for the experimental data obtained with 90 and 340 μW excitation power. The wavelength amplitude dependency of the retrieved time components (besides IVR) for the measurement sets at 45 and 340 μW excitation is plotted in Figure 6.

An extra decay time component of 110 ps starts to show up at 90 μW and more clearly at 340 μW. The wavelength dependence of the amplitude of this component has a shape similar to that of the amplitude of the 2.2-ns component and varies with increasing power as illustrated in Figure 7. A dominant change in amplitude distribution is only present in the 510-nm and 570−730-nm regions, and the amplitude behavior is similar for different excitation powers (for details of the transient absorption data, see SI Figure 3).

PhCN. PI-(pPh)$_3$-PI shows a very low fluorescence signal in the highly polar solvent PhCN. Femtosecond transient

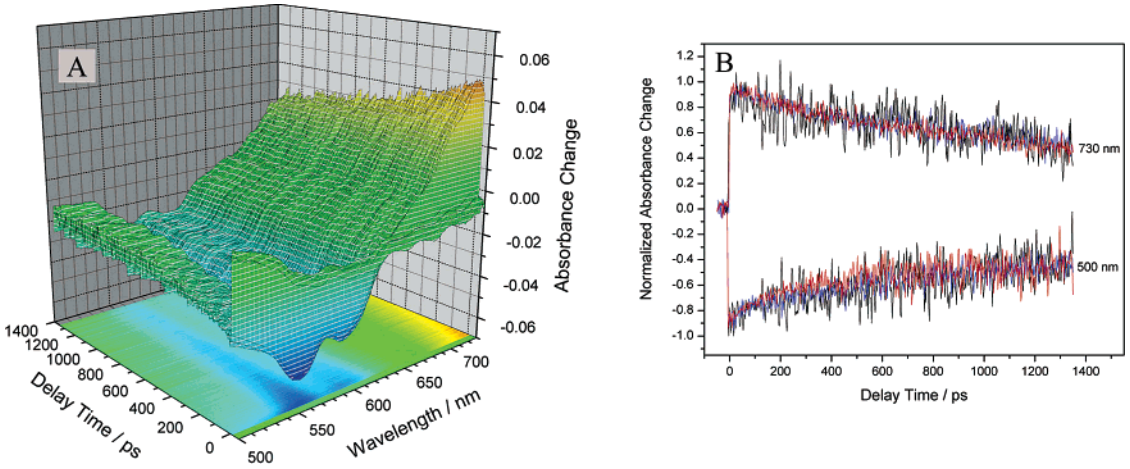

Figure 4. Three-dimensional plot of the femtosecond transient absorption spectra of **PI-(pPh)$_3$-PI** in MCH (A). Decay traces recorded in MCH (B) with excitation power of 60 μW (black), 120 μW (blue), and 340 μW (red) in a 1400-ps time window. The wavelengths were selected according to the regions of interest.

absorption experiments revealed a kinetic behavior remarkably different from that found in the previous solvents (Figure 8A). The positive band centered at 630 nm is formed slower and decays faster; a faster decay is also observed for the negative signal at 500 nm or the positive one at 730 nm. The global kinetic analysis shows that, in addition to IVR and vibrational relaxation, two components with decay times of 35 and 350 ps are retrieved that appear not to be affected by the change in excitation power as seen in Figure 8B, where traces recorded with excitation powers of 60, 120, and 340 μW are compared (see SI Figure 4 for transient absorption traces, corresponding fits, and the wavelength dependency of the partial amplitudes).

For an overview of the data recorded in different solvents for **PI-(pPh)$_2$** and **PI-(pPh)$_3$-PI**, the decay time constants found in both SPT and transient absorption experiments are compiled in Table 2. In all femtosecond data, two components of IVR and VR were found additionally but not included in the table, vide supra.

Discussion

Stationary Measurements. The **PI-(pPh)$_2$** absorption spectrum consists of two different regions. The blue part (350−450 nm) of the spectrum is related to the absorption of **pPh** units, and its intensity is proportional to the number of these units. Well separated from that, the band centered at 520 nm is due to the S_0–S_1 transition of the **PI** subsystem. This band appears unstructured compared to the absorption of the phenyl-substituted chromophore (**C1P1**) as a result of some ground-state delocalization over the first **pPh** moiety.[7] Its extinction coefficient measured in toluene is 37% higher than the corresponding one of **C1P1**. Only a small red shift is observed in tetralin ($n = 1.54$) compared to that in MCH ($n = 1.42$) due to either an increase in the effect of the electronic polarizabillity of these solvents (refractive indices taken from reference[37]) or an increased stabilization of the excited state with a small CT character by the more polar tetralin. The maximum (570 nm) and vibronic features of the emission spectrum of the **PI-(pPh)$_2$** in MCH are only weakly shifted with respect to those of **C1P1** in toluene. This suggests that, in apolar solvents, after geometrical relaxation the excited state involved in the fluorescence has a dominant local character (i.e., is mainly centered on **PI**). This is supported by the quantum-chemical calculations, vide infra. Upon increasing the solvent polarity from MCH to tetralin and THF, the maximum of the emission band shifts to longer wavelengths and becomes broader while the fine structure fades out. In tetralin and THF, the relaxed excited state becomes delocalized over the neighboring pentaphenylene unit and obtains the spectroscopic character of a CT-like species. Furthermore, the gradual decrease of the quantum yield from 0.90 (MCH) to 0.53 (tetralin) and 0.35 (THF) points to an increased efficiency of the radiationless deactivation of the relaxed singlet excited state in a more polar solvent. It should be emphasized at this point that the occurrence of an intramolecular charge transfer has previously been reported in a similar molecular system **PI-(pPh)$_1$** (containing a single **pPh**) unit in THF as solvent.[35]

The system **PI-(pPh)$_3$-PI** shows similar stationary absorption and emission spectra, except for the smaller ratio between the absorption intensities of the two subsystems at the respective maxima. In the most polar solvent PhCN, both absorption and emission feature a bathochromic shift. This suggests that the Franck−Condon excited state as well as the relaxed excited state responsible for the emission in PhCN show a dipole character which, considering the larger shift of the emission compared to the absorption, is more pronounced in the relaxed excited state. Similar to **PI-(pPh)$_2$**, the quantum yield (Table 1) undergoes an expected decrease upon raising the solvent polarity. However, this decrease is slightly larger in a more polar solvent, suggesting the occurrence of a slightly more efficient nonradiative process in the excited state due to the presence of three **pPh** units. No shift of the emission spectrum can be observed if one compares **PI-(pPh)$_2$** to **PI-(pPh)$_3$-PI** in the same solvent, indicating the contribution of a charge transfer state is identical for both compounds in the same solvent.

SPT and Femtosecond Transient Absorption. PI-(pPh)$_2$. The larger extinction coefficient of 52 000 M^{-1} cm^{-1} with respect to **C1P1** and the faster decay time of 2.8 ns versus 4.2 ns at the same emission maximum suggest an enhanced transition dipole moment as a result of conjugation between the nearly collinear **PI** (the S_0–S_1 transition dipole oriented along the long axis) and the **(pPh)$_2$** moieties.

MCH and Tetralin. In the transient absorption data recorded in MCH (Figure 2A), two bands characteristic for the **PI**

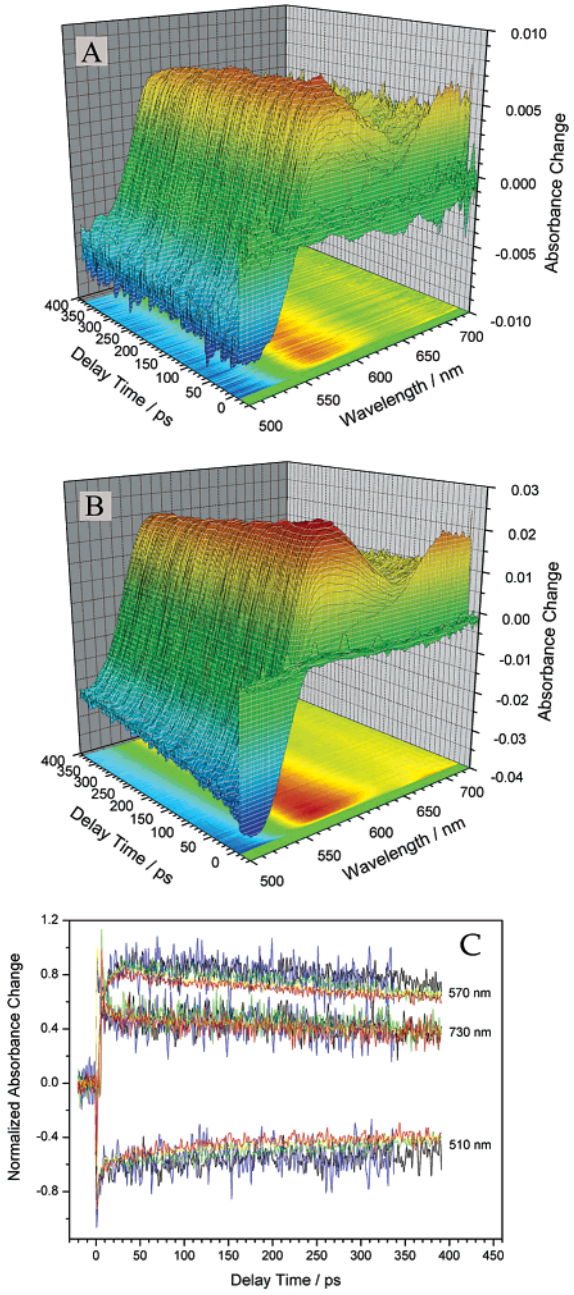

Figure 5. Comparison of the three-dimensional plot of the femtosecond transient absorption spectra of **PI-(pPh)$_3$-PI** in THF recorded with 45 μW (A) and 120 μW (B) excitation power. Comparison of the decay traces of the femtosecond transient absorption of **PI-(pPh)$_3$-PI** in THF recorded with increasing excitation power 45 (black), 60 (blue), 90 (green), 120 (yellow), and 340 μW (red) for three wavelengths of interest (C).

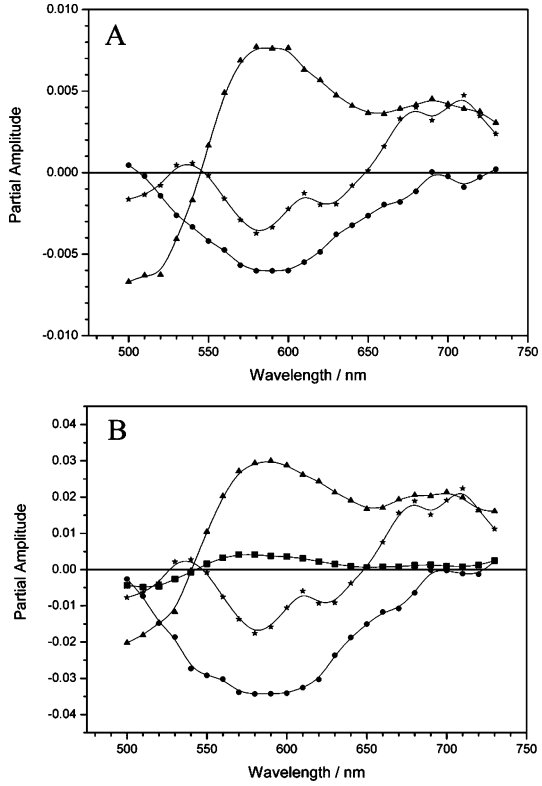

Figure 6. Wavelength dependence of the partial amplitudes of the decay times obtained by global analysis of the decays of the femtosecond transient absorption of **PI-(pPh)$_3$-PI** in THF with two excitation powers of 45 μW (A) and 340 μW (B): 4.2 ps (∗), 6 ps (●), 110 ps (■), and 2.2 ns (▲).

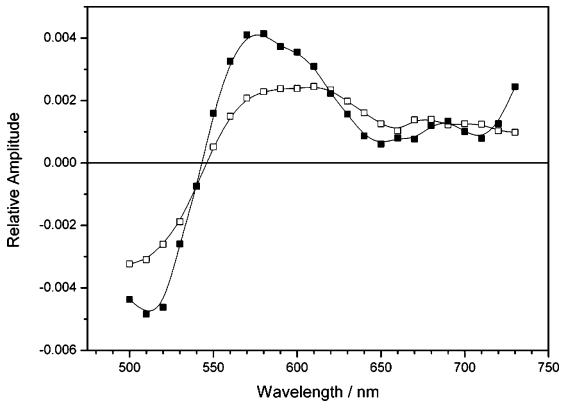

Figure 7. Wavelength dependence of the partial amplitudes of the 110-ps decay time obtained by global analysis of the decays of the femtosecond transient absorption of **PI-(pPh)$_3$-PI** in THF with excitation power of 90 μW (□) and 340 μW (■).

chromophore rise instantaneously after excitation and decay concurrently on a nanosecond time scale. The negative part of the signal has two origins: in the 500−550-nm region it is due to ground-state depletion mainly resembling the steady-state absorption while the stronger band at 540−650 nm is associated with stimulated emission fully matching the stationary emission spectra. The positive part (650−730 nm) with a molar extinction coefficient comparable to the value for the depletion band corresponds to the S_1–S_n absorption band within the **PI** chromophore. This is 30 nm bathochromically shifted as compared to the one corresponding to **C1P1** in toluene. No apparent band shift is reproduced on the bottom plane projection, neither within this time interval nor in 50 ps (data not shown). Though the zero crossing point (650 nm) is well-defined, due to the two signals opposite in sign which cancel each other, the excited-state absorption might extend to lower wavelengths while the induced emission will extend beyond 650 nm.

The femtosecond measurements in tetralin appear different since a new band, best identified in the bottom-projection plane of the 3D figure, appears at time zero and decays within 150 ps. At longer time, the transient absorption exhibits a broader negative band as compared to the corresponding one in MCH. This is the joint result of the ground-state bleaching that is 10 nm red-shifted (resembling the stationary absorption Figure 1 A) and the strong stimulated emission from the LES of the **PI** chromophore (560 nm) as it was found in MCH. The bands are only adjacent immediately after the excitation process. Within

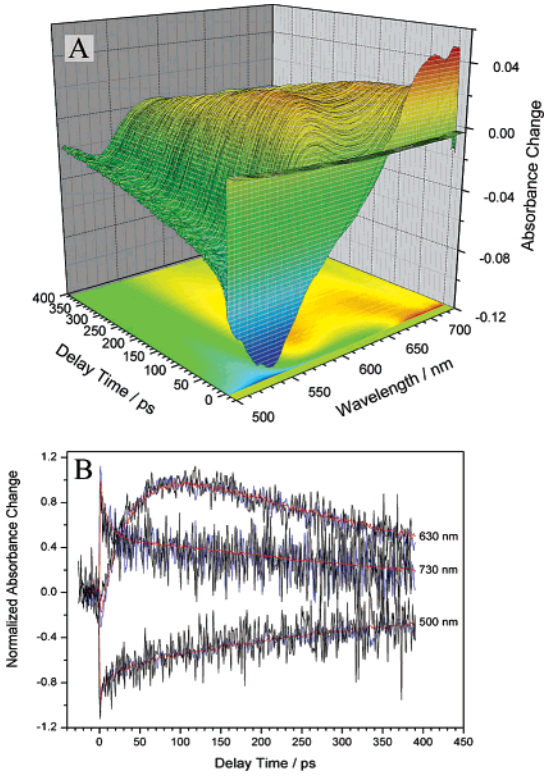

Figure 8. Three-dimensional plot of the femtosecond transient absorption spectra of **PI-(pPh)$_3$-PI** in PhCN (A) and decay traces recorded in PhCN (B) with excitation power of 60 μW (black), 120 μW (blue), and 340 μW (red) in the 420-ps time window. The wavelengths were selected according to the regions of interest.

the first 150 ps, the stimulated emission signal from the LES decreases and a new signal increases at a longer wavelength (580 nm), indicating the evolution of the emitting state. From stationary data, the kinetic analysis of the time-resolved data, and the interpretation of these bands observed in transient absorption spectroscopy, we suggest that a new state is formed with a time constant of 52 ps from the LES. This state corresponds to an intramolecular charge transfer-like (CT-like) state that is due to an electronic shift from the **pPh** subsystem to the excited **PI** chromophore. Note that the weak absorption of this newly formed state is superimposed to the stronger signal of the stimulated emission.

THF. The SPT experiments on **PI-(pPh)$_2$** in the more polar solvent THF reveal a two exponential fluorescence decay with time constants of 2.2 ns (4.5×10^8 s^{-1}) and a shorter one (<30 ps). However, this could not explain the quenching process leading to a drop of the quantum yields to 35%. When the **PI-(pPh)$_2$** system is measured in femtosecond transient absorption, the three-dimensional spectra clearly look different from those in MCH and even in tetralin. Figure 2B shows a three-dimensional plot of the transient absorption spectra of **PI-(pPh)$_2$** in THF recorded within the smallest time window (50 ps). The main difference is a positive band that appears at 550 nm immediately after excitation and rises in about 20 ps while apparently shifting 20 nm to the red part of the spectrum. Its absorption intensity grows in time at the expense of the excited-state absorption at 730 nm, which decays with the same time constant. This new band is strong evidence for the creation of a species that resembles the spectral properties of a radical anion of the **PI** chromophore for which maxima at 600 and 620 nm were reported previously in molecular systems containing **PI**s in different solvents.[2,9,11,35] In spite of the important CT character of this newly formed species, suggested by a well-defined positive signal around 550 nm, the absorption at 730 nm has not decayed completely after 40 ps. The remainder must be attributed to the pentaphenylene radical cation-like absorption band (of the decay ratio to about 20%) that grows in time at the same rate as the anion-like band does. It has previously been observed experimentally that the added anion-like and cation-like absorptions form a broad band between 550 and 700 nm.[35] This newly formed state could be responsible for the 2.2-ns fluorescence signal detected in SPT. As the state with CT character is formed hundred times faster (6 ps) than the decay of the LES in MCH or tetralin, it must be reached with a quantum yield exceeding 99%. In fact, due to the limited time resolution of the SPT setup, the fast CT-like formation time constant (about 6 ps) was not resolved in SPT. Putting side by side the transient absorption data obtained in MCH or tetralin, the ground state is recovered faster in THF (Figure 3), indicating that decay of the CT-like state directly repopulates this last state. From steady-state and transient absorption data, one can observe a good overlap between the stationary emission of the CT-like state of **PI-(pPh)$_2$** and its absorption band to higher excited states (see SI for details).

PI-(pPh)$_3$-PI. MCH and Tetralin. The three-dimensional plot of the transient spectra of **PI-(pPh)$_3$-PI** in MCH recorded in a longer 1400-ps time window (Figure 4A) looks very similar to those of the **PI-(pPh)$_2$**. The identical position and shape of the ground-state depletion (500−550 nm), stimulated emission (540−650 nm), and S_1–S_n absorption (650−730 nm) bands can be seen.

By comparing the decay traces (Figure 4B) recorded with pump power of 60, 120, and 340 μW, an almost perfect match is found in both depletion and excited-state absorption bands. Thus, independent of the excitation power, these bands decay with the same rates as the ones found for the **PI-(pPh)$_2$** compound. This indicates that although both chromophores can be excited by the same femtosecond laser pulse, no annihilation process takes place here.

It has been shown above that for **PI-(pPh)$_2$** the relaxation to a CT-like state does occur in tetralin. The same is found for **PI-(pPh)$_3$-PI** in the same solvent. Like for the **PI-(pPh)$_2$** compound, during the first 150 ps after excitation, the negative signal evolves into two individual bands that perfectly coincide with the ground-state absorption and CT-like state emission bands. If the normalized steady-state absorption band is subtracted from the negative transient absorption band, the resulting stimulated emission signal clearly demonstrates a red shift that can be related to the mixing of the LES with a CT state. By reducing the excitation pump power from 340 to 60 μW, the traces recorded in the 420-ps time window stay almost identical, suggesting that no interaction occurs between the locally excited states within the excited **PI**s or between the mixed LE/CT-like states (for further details, see SI Figure 2).

THF. PI-(pPh)$_3$-PI in THF shows a fast evolution from the LES to a CT-like state (resembling the spectral properties of an intramolecular charge transfer state), quickly recognized by the rise of the band localized in the 550−650 nm region (Figure 5A). Upon stepwise increase of the excitation power impinging on the sample between 45, 60, 90, 120, and 340 μW, a clear

Table 2. Decay Time Components (in Picoseconds) Obtained by SPT (λ_{exc} = 483 nm, λ_{det} = 560, 590, 620, 650, and 680 nm) and Femtosecond Transient Absorption Experiments

solvent	MCH		tetralin		THF			PhCN	
compound	τ_1	τ_2	τ_1	τ_2	τ_1	τ_2	τ_3	τ_1	τ_2
PI-(pPh)$_2$	—[c]	2800	52	2600	6	2200	—[c]	nd[a]	nd[a]
PI-(pPh)$_3$-PI	—[c]	2700	50	2600	6	2200	110[b]	35	350

[a] Not determined. [b] Appeared only at high excitation power. [c] Not found.

and systematical difference is observed in both the CT-like absorption and ground-state depletion band. When increasing the excitation power, the CT-like absorption band decays faster and the ground state (negative band) is recovered more rapidly (Figure 5B).

Figure 5C displays a view of the time-dependent behavior of these bands, comparing the traces recorded in three sections across the wavelength axis at 510 nm (ground-state depletion), 570 nm (CT-like formation and decay), and 730 nm (S_1–S_n absorption). In contrast to the data obtained from the **PI-(pPh)$_2$** compound in THF, it is obvious that upon increasing the excitation power both CT-like and depletion bands decay faster, whereas the traces at 730 nm remain almost unaffected. The small change is due to the remainder of the radical cation-like absorption signal that overlaps with the excited-state absorption band. This implies that the relaxation of the LES population of the **PI** is independent of the excitation power while the other two transitions are directly affected.

While the 4.2-ps component that is also found for the **PI-(pPh)$_2$** is attributed to vibrational/solvent relaxation within the **PI** chromophore, the decay of 6 ps (1.66×10^{11} s^{-1}) is attributed to the formation of the CT-like state (Figure 6A). This 6-ps time component shows a negative amplitude behavior covering the entire **PI** anion-like and **(pPh)$_3$** cation-like absorption band. The long component of 2.2 ns displays a negative amplitude between 500 and 540 nm, indicating ground-state repopulation, whereas the positive part beyond 540 nm shows the CT-like state decaying with this time constant. Both these components show that the **PI** anion-like and **(pPh)$_3$** cation-like bands are well extended over a 550−730 nm spectrum which is otherwise hidden in the three-dimensional plot. The excited-state absorption band appears to decay with the VR time constant. However, in that region the signal must have an important contribution of the 6-ps component which is difficult to separate by the fit procedure.

The same kinetic analysis has been carried out for the experimental data obtained with 90 and 340 μW excitation power. The wavelength amplitude dependency of the time components for the 340 μW measurements set is plotted in Figure 6B. Already at 90 μW and more pronounced at 340 μW (Figure 6 B), an extra decay time component of 110 ps (9×10^9 s^{-1}) can be extracted. It features a negative amplitude in the depletion region and a positive one at the part of the spectrum where the radical anion-like band decays. Hence, a fraction of the population in the CT-like state undergoes an additional deactivation process with a time constant of 110 ps, and a part of it is recovered in the ground state.

This partial amplitude is increasing with the pump power as more **PI** chromophore pairs are excited simultaneously (Figure 7). Such behavior unambiguously indicates that this process is related to an interaction between the two CT-like states formed within the end-capped **PI**s; the **PI-(pPh)$_2$** compound in the same solvent showed neither this extra component nor power-dependent characteristics. This process appears only in the presence of the second chromophore, strongly supporting its attribution to an annihilation between the two excited chromophores.

PhCN. In the most polar solvent, PhCN, both ground-state depletion and radical anion-like absorption bands are 10 nm red-shifted compared to THF (Figure 8A). For the ground-state absorption band, this suggests a further stabilization of the Franck−Condon excited state induced by the solvent. The kinetic analysis of these traces shows that the formation of the CT-like state occurs with a smaller time constant (35 ps, 2.85×10^{10} s^{-1}), while the recombination time becomes faster (350 ps, 2.8×10^9 s^{-1}) compared to THF. Since for a solvent of higher polarity the formation of the CT-like state slows down compared to THF, the observed process must be a consequence of an intrinsic property of PhCN. Due to its higher viscosity (1.267 mPa·s compared to 0.45 mPa·s for THF), the geometrical relaxation and solvent relaxation occur on a longer time scale which will diminish the rate of the formation of the CT-like state.[37]

In PhCN, **PI-(pPh)$_3$-PI** forms a CT-like state resembling the one observed previously in molecular systems containing **PI**s (at the same wavelength region; see SI Figure 4 for more details) and characterized by dominant nonradiative processes ($k_{nr} = 2.8 \times 10^8$ s^{-1}, $k_r = 5.7 \times 10^6$ s^{-1}), which explains the low quantum yield reported in Table 1.[2,9,11,35] The formation of the CT-like state is rapidly followed by a fast internal conversion process (with which charge recombination is associated), which is in competition with a (slower) parallel CT−CT annihilation. Indeed, by comparing the traces in the three regions corresponding to ground-state depletion, CT-like absorption, and LES absorption bands, no excitation power dependence is observed (Figure 8B).

The femtosecond transient absorption results allowed the following conclusions for **PI-(pPh)$_2$** and **PI-(pPh)$_3$-PI**: upon increasing the solvent polarity from low to medium (tetralin and THF), a new relaxation pathway of the LES occurs that involves the formation of a new (CT-like) emitting excited state. Although THF is a more polar solvent but less viscous (0.45 mPa·s) than tetralin (2.2 mPa·s), the geometrical relaxation (the decrease in the planar angle between the **PI** and **pPh** units) develops on a shorter time interval due to a smaller internal resistance which leads to an increased rate of the CT-like formation from 1.9×10^{10} s^{-1} (tetralin) to 1.66×10^{11} s^{-1}.[37] The transient spectra enabled us to establish the spectral positions and the amplitude of the S_1–S_n absorption bands of the locally excited state and the CT-like state for different solvents. In MCH, a small overlap is found between the stationary emission spectra and the locally excited-state absorption. Tetralin as a mildly polar solvent provides a larger overlap

of emission and absorption of the CT-like state but a slower charge transfer state formation. In addition to such a process, in THF a very fast and efficient formation of the CT-like state is experimentally found.

Quantum-Chemical Calculations. To assess the amount of excited-state delocalization over the phenylene-based arm, it is useful to compare the results of INDO/SCI excited-state calculations performed on both the AM1 (AM1-CI) ground-state and excited-state geometries of the compound **PI-(pPh)$_3$** and the unsubstituted perylene monoimide **PI**. The transition density distributions show delocalization (local map of the transition dipole moment) for the S_0–S_1 excitation in the two compounds, as calculated on the basis of their relaxed S_1 equilibrium geometry (see SI Figure 5 for details). Note that the same picture also holds in the ground-state S_0 configuration, probably because the confinement on the **PI** unit driven by the photoinduced structural deformations (electron−phonon coupling) is compensated by the stronger coupling between the **PI** and **pPh** entities associated with a smaller torsion angle in the excited state (∼50° in S_1 compared to ∼61° in S_0). In both cases, the transition densities are mostly confined on the **PI** moiety, however, with some contributions of the neighboring **pPh** unit in **PI-(pPh)$_3$**. This results in a slight red shift of the lowest optical excitation (by ∼0.1 eV) upon going from **PI** to **PI-(pPh)$_3$** and, most importantly, a ∼45% increase in the transition dipole moment; these predictions are consistent with the measured bathochromic shift and the 37% higher extinction coefficient in **PI-(pPh)$_3$** as compared to that in **C1P1**.

Next, we applied the same INDO/SCI calculations for different screened potentials ($\sigma > 1$) to mimic solvents with increasing polarity. As a test for the crude model used to account for solvent effects, we studied the evolution with σ (see Quantum-Chemical Calculations Methodology section) of the S_1–S_0 vertical transition energy in the (gas-phase) excited-state equilibrium geometry. As expected, the calculations yield a decrease in the excitation energy when σ gets larger, which is accompanied by an increased charge-transfer character of the lowest excited state (see SI Figure 6 for details). This red shift of ∼0.45 eV when going from $\sigma = 1$ to $\sigma = 4$ compares reasonably to the observed shift in fluorescence maximum upon switching from apolar to polar solvents (e.g., the bathochromic displacement amounts to 0.3 eV when going from MCH to THF). The increased charge-transfer character is accompanied by a reduced transition dipole moment, but the effect is small (∼10% decrease from $\sigma = 1$ to $\sigma = 4$) and so is the impact on the efficiency of the CT−CT annihilation, vide infra.

Excited-state wavefunction analyses were performed to quantify the amount of charge-transfer character in the S_1 excited state. Figure 9A shows the changes in atomic charge density when going from the ground state to the excited state of the **PI** alone as well as in **PI-(pPh)$_3$**. It is clearly seen that for σ values representing polar solvents the lowest excited state displays a pronounced charge-transfer character with negative charge density on the **PI** unit and positive charge density on the neighbor **pPh** pentamer. This is further illustrated in Figure 9B where the contributions from charge transfer and local excitations to the computed two-particle electron−hole wavefunctions are reported.[48]

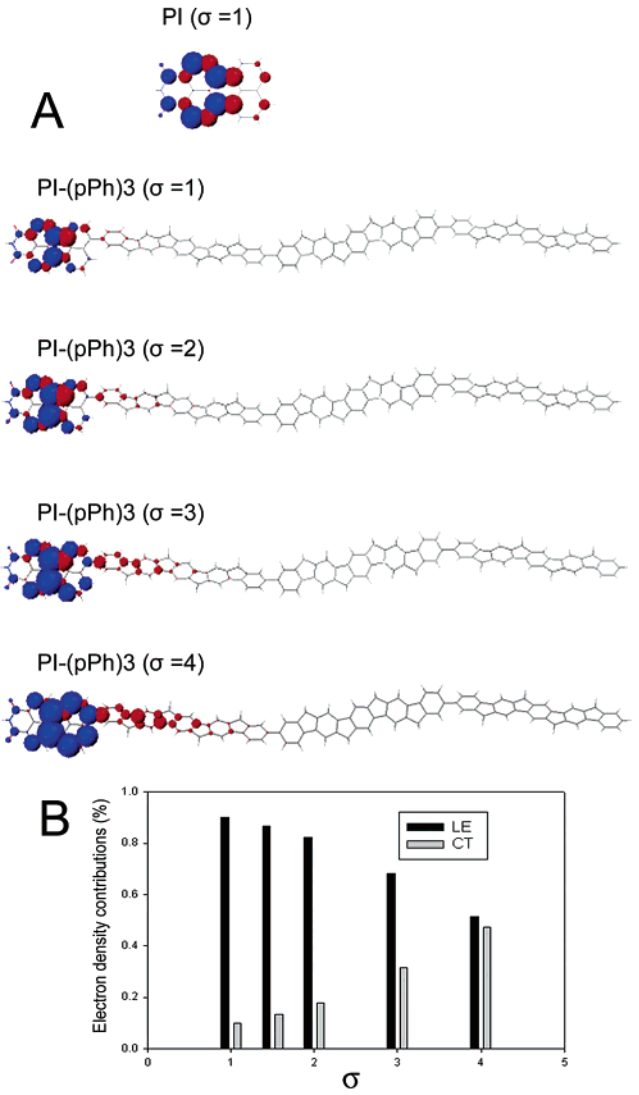

Figure 9. (A) Changes in atomic charge density when going from the ground-state S_0 to the lowest singlet excited-state S_1, as computed at the INDO/SCI (ZDO) level for **PI** and **PI-(pPh)$_3$** for different σ values (on the basis of the AM1/CI gas-phase excited-state geometries). (B) Contributions from local (LE) and charge transfer (CT) excitations to the S_1 electron−hole wavefunction, as calculated in the relaxed excited-state geometry of **PI-(pPh)$_3$**.

Modeling. PI-(pPh)$_3$-PI in THF shows a bichromophoric interaction validated by the change of the excitation power and comparison with the **PI-(pPh)$_2$** system. This annihilation must be viewed as an energy-transfer process between the end-capped chromophores simultaneously promoted into their lowest singlet excited states (S_1). Within such a process, one **PI** transfers its excitation energy to the second **PI** returning to the ground state while the second one uses the additional energy to reach a higher-lying excited state (S_n). As an end result, the S_1 excitations get quickly annihilated while a fraction of the population is recovered in the ground state.

As experimentally proven above, the excitation energy transfer can take place between the LESs but can also involve singlet CT states formed. To find the conditions, we need a closer look at the singlet−singlet annihilation well described by the Förster mechanism.[49] Table 3 provides the calculated

(48) Rissler, J.; Bässler, H.; Gebhard, F.; Schwerdtfeger, P. *Phys. Rev. B* **2000**, *64*, 045122.

(49) Förster, T. *Discuss. Faraday Soc.* **1959**, *27*, 7−17.

Table 3. Calculated Chromophore Physical Separation and Förster Distances, Overlap Integrals, Rate Constants, and Annihilation Efficiencies for **PI-(pPh)$_3$-PI**

annihilation type	R (nm)	R_0 (nm)	$J(\upsilon)$ $\times 10^{-14}$ (cm^{-6} mol^{-1})	k_{ann} $\times 10^7$ (s^{-1})	η_{ann} (%)
LES−LES	7.4	5.0	2.3	4.8	12
CT−CT	5.4	7.5	64	320	88

values for R, R_0, $J(\upsilon)$, k_{ann}, and η_{ann} for both LES−LES and CT−CT annihilation processes based on the spectral overlap LES−LES and CT−CT (see SI for details of calculations and Figure 8 for graphical date).

According to the estimations compiled in Table 3, the annihilation process occurs with low efficiency between LES (12%) and higher efficiency between CT states (88%) as a result of a larger overlap integral and a shorter critical distance. Although an inefficient LES−LES annihilation is predicted by the calculation, such an interaction was not observed. The lack of annihilation in MCH and tetralin is consistent with the interchromophoric separation distance that has been not reduced.

Quantum-chemical investigations performed on **PI-(pPh)$_2$** confirmed the conformational change going on upon relaxation in the LES (change in the twisting angle between the **PI**-endcap moiety relative to the **pPh** unit). This configurational relaxation yields an enhanced electronic coupling between the **pPh** donor and the **PI** acceptor; as a consequence, the lowest excited state acquires a substantial (solvent-dependent) CT character and extends up to about 1 nm over the adjacent **pPh** subsystem. At the same time, the excited-state absorption transition dipole moment has a significantly high value shown by the intense CT-like absorption band in transient absorption (Figure 5) and supported by the quantum-chemical calculations (SI Figure 6). Note that the excited-state absorption band undergoes a blue shift in solvents of higher polarity such as THF and PhCN. Due to this blue shift from 730 (MCH) to 700 nm (PhCN), the energetic position of the excited-state absorption resembles that of a **PI** radical anion (SI Figure 7). The small intensity of the stimulated emission of the LES signal in THF implies that, after geometrical relaxation, the formation of the CT-like state (6 ps) occurs almost in parallel to the vibrational/solvent relaxation processes. If then both **PI**s simultaneously form CT states in **PI-(pPh)$_3$-PI**, the effective dipole−dipole distance is reduced from 7.4 nm to about 5.4 nm, providing a significant benefit for the annihilation efficiency (vide supra). Additionally, a better match of the CT absorption (570 nm) and emission (630 nm) bands yields a larger overlap integral compared to the corresponding one in MCH (see Table 3 and SI for details). As a net result, the dipole−dipole separation distance becomes smaller than the Förster radius, thus strongly enhancing the efficiency of the annihilation. Note, however, that the experimentally observed efficiency is smaller, which might be related to the number of excitation photons available per molecule in our femtosecond experiments.

Conclusions

The femtosecond time-resolved transient absorption data presented here clearly demonstrate that in the rigid perylene end-capped polyphenylenes **PI-(pPh)$_3$-PI** a CT−CT annihilation takes place after formation of two independent CT-like states. This complex event is expressed in a solvent of medium polarity by comparing the transient decay traces recorded with five different excitation powers in three spectral regions corresponding to ground-state depletion, CT-like, and locally excited-state absorption band. Furthermore, in **PI-(pPh)$_2$** no power dependency has been found, strongly indicating that this process is credited to an excited-state bichromophoric interaction. By selecting the right solvent, the CT-like state is formed fast (6 ps) and efficiently and lives long enough (2.2 ns) to allow the competition of a kinetic process with a time constant of 110 ps. Quantum-chemical calculations show that the excited-state wavefunction significantly spreads over the neighboring pentaphenylene skeleton in polar solvents and diminishes the center-to-center separation distance by about 2 nm.

The single-molecule anti-bunching data that suggested that CT-like states were involved are now experimentally confirmed by the data presented in this study.[27] The CT−CT annihilation suggested has been directly proven by the detailed series of SPT and femtosecond transient absorption experiments.

Acknowledgment. Support from the FWO, the Flemish Ministry of Education (GOA 2001/02, GOA 2006/2, ZWAP 04/007), and the BMBF, the Federal Science Policy of Belgium (IAP-V-03), is acknowledged. A Max Planck research award and an Eurocores grant (ESF-Bionics) are also acknowledged.

Supporting Information Available: Details of femtosecond transient absorption traces including the fits, quantum-chemical calculations, calculation for chromophore separation distance, spectral overlap, overlap integrals, critical distances, rate constants, and efficiencies of annihilation. This material is available free of charge via the Internet at http://pubs.acs.org.

JA064794E